Geophys. J. Int. (2004) **156,** 129–139 doi: 10.1111/j.1365-246X.2004.02126.x

Estimating tectonic history through basin simulation-enhanced seismic inversion: geoinfomatics for sedimentary basins

Kush Tandon,[1,*,†] Kagan Tuncay,[1] Kyle Hubbard,[1] John Comer[2] and Peter Ortoleva[1]

[1]*Laboratory for Computational Geodynamics, Department of Chemistry, Indiana University, Bloomington,* IN 47405-7102, *USA.*
E-mails: ktuncay@indiana.edu; ortoleva@indiana.edu
[2]*Indiana Geological Survey,* 611 *North Walnut Grove, Bloomington,* IN 47405-2208,*USA*

Accepted 2003 September 10. Received 2003 September 1; in original form 2002 December 3

SUMMARY

A data assimilation approach is demonstrated whereby seismic inversion is both automated and enhanced using a comprehensive numerical sedimentary basin simulator to study the physics and chemistry of sedimentary basin processes in response to geothermal gradient in much greater detail than previously attempted. The approach not only reduces costs by integrating the basin analysis and seismic inversion activities to understand the sedimentary basin evolution with respect to geodynamic parameters—but the technique also has the potential for serving as a geoinfomatics platform for understanding various physical and chemical processes operating at different scales within a sedimentary basin.

Tectonic history has a first-order effect on the physical and chemical processes that govern the evolution of sedimentary basins. We demonstrate how such tectonic parameters may be estimated by minimizing the difference between observed seismic reflection data and synthetic ones constructed from the output of a reaction, transport, mechanical (RTM) basin model. We demonstrate the method by reconstructing the geothermal gradient. As thermal history strongly affects the rate of RTM processes operating in a sedimentary basin, variations in geothermal gradient history alter the present-day fluid pressure, effective stress, porosity, fracture statistics and hydrocarbon distribution. All these properties, in turn, affect the mechanical wave velocity and sediment density profiles for a sedimentary basin. The present-day state of the sedimentary basin is imaged by reflection seismology data to a high degree of resolution, but it does not give any indication of the processes that contributed to the evolution of the basin or causes for heterogeneities within the basin that are being imaged. Using texture and fluid properties predicted by our Basin RTM simulator, we generate synthetic seismograms. Linear correlation using power spectra as an error measure and an efficient quadratic optimization technique are found to be most effective in determining the optimal value of the tectonic parameters. Preliminary 1-D studies indicate that one can determine the geothermal gradient even in the presence of observation and numerical uncertainties. The algorithm succeeds even when the synthetic data has detailed information only in a limited depth interval and has a different dominant frequency in the synthetic and observed seismograms. The methodology presented here even works when the basin input data contains only 75 per cent of the stratigraphic layering information compared with the actual basin in a limited depth interval.

Key words: complex systems, data assimilation, geoinfomatics, geothermal gradient, sedimentary basin modelling.

1 INTRODUCTION

One of the challenges for understanding a complex system that evolves over millions of years, such as a sedimentary basin is the very poor constraint on parameters that govern or significantly affect the physical and chemical processes operating in a sedimentary basin. In a typical approach studying the physics and chemistry

*Present address: College of Oceanic and Atmospheric Sciences, Oregon State University, Corvallis, OR 97331-5503. E-mail: kush@coas.oregonstate.edu
†To whom the correspondence should be addressed.

involved in the formation of sedimentary basins either in an academic or industrial setting, seismic inversion and basin modelling are essentially carried out as independent activities. Even when information from seismic inversion is used, it is only a small part of the basin modelling effort and it does not attempt to capture the richness and diversity of processes involved. However, a comprehensive basin reaction, transport, mechanical (RTM) numerical model makes predictions concerning fluid and rock property distributions that could, in principal be used to enhance the quality of seismic inversion. It is the objective of this study to integrate and automate the seismic inversion and basin modelling efforts into a cost-effective technology that enhances the quality and general information content of both. Also, one of the fundamental problems in performing inversion in earth sciences is the lack of enough detailed information concerning the Earth to make predictions that can be tested with confidence using various data sets. Therefore, it is an important issue to lay down the theoretical framework for methodology for detailed predictions for the evolution of the outermost veneer of the Earth's crust, the sedimentary basins, and approaches for basin data assimilation.

Evolution of a sedimentary basin depends on the strong coupling among many processes (hydrocarbon generation, fracturing, compaction, etc.). Tectonic parameters (such as geothermal gradient and extension/compression histories) strongly affect these physical and chemical processes. Uncertainties in the input parameters needed to run a basin model, therefore, lead to uncertainties in the predictions. Here, a method is presented to constrain these uncertain tectonic parameters to arrive at a higher resolution geophysical imaging tool by integrating reflection seismology data and RTM basin modelling. In Fig. 1, we suggest how this approach can be automated in a highly parallelizable, automated computational approach.

Reflection seismic data are commonly used to delineate the sedimentary basin architecture, structural evolution and sedimentary process as it is a very high-resolution, geophysical subsurface imaging technique (McQuillin *et al.* 1984). However, seismic reflection data alone cannot discriminate amongst many factors that cause the acoustic impedance contrast (e.g. gas saturation, finely laminated sediments and gouge) imaged by reflection seismology. A limitation of many conventional geophysical techniques is that they are not robust and are fraught with subjective interpretation.

Seismic inversion is often used to determine rock and fluid properties (composition, fracture intensity and orientation, fluid saturation and overpressure). Most seismic inversion techniques limit their analysis to a small set of variables to allow invertibility of the seismic reflection data. For example, Mallick *et al.* (1998) used the amplitude variation with offset technique to predict fracture orientations. Ramos & Davis (1997) studied the detection of fracture density variations by delineating zones of large Poisson ratio contrasts. These and other studies (Cabrera 1996; Boadu 1998) show that predictions using reflection seismology are limited to a few rock properties. We suggest that seismic interpretation and our understanding of sedimentary basins can be greatly enhanced through the integration of comprehensive basin modelling (Tuncay *et al.* 2000a,b; Tuncay & Ortoleva 2001, 2003) and reflection seismic data. We have no knowledge of a previous attempt to study the complex evolution of heterogeneities that act as acoustic impedance contrasts and the interaction of tectonics from a comprehensive basin modelling approach. Our objective is to develop a technology that will enable us to estimate a set of basin parameters constrained by the observed reflection seismic data. This could allow us to aid the remote detection of economically important fractured compartments and conventional reservoirs as well as the estimation of tectonic conditions to which the basin was subjected.

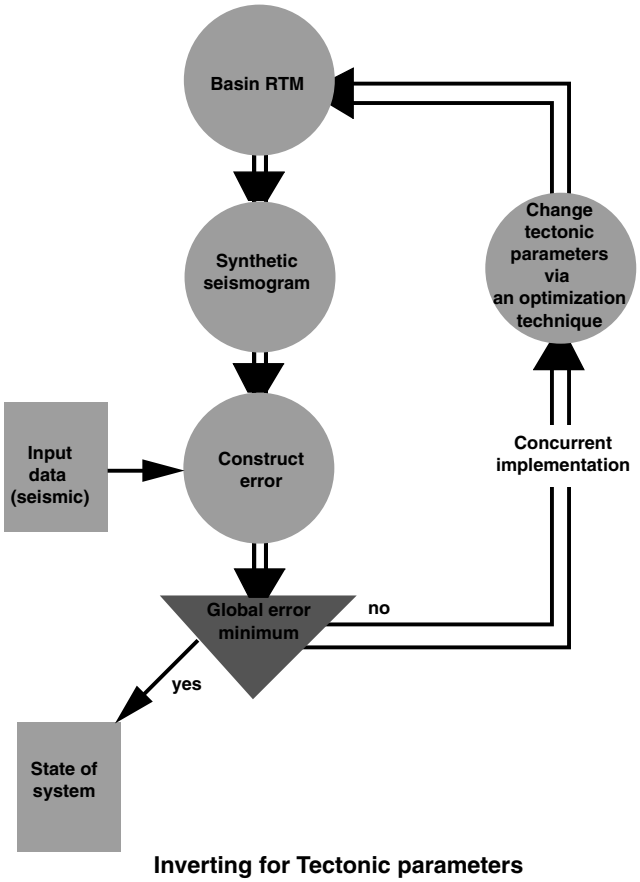

Figure 1. A flow chart for estimating the tectonic parameters automatically through our seismic inversion-basin modelling algorithm. This technique has been implemented in a parallel fashion through a common error database, as shown.

As a demonstration of our technique, the geothermal gradient is estimated using a comprehensive simulator, Basin RTM (Tuncay *et al.* 2000a,b; Tuncay & Ortoleva 2001, 2003) and reflection seismic data. In this study we use a Basin RTM simulated synthetic seismogram at 30 $^{\circ}$C km^{-1} geothermal gradient as the 'observed' data to evaluate the vulnerability of the approach to noise and incomplete data (Fig. 2). The following issues are investigated.

(1) The choice of error measure and its robustness to noisy observed data.

(2) The performance of the technique when a complete, detailed description of the stratigraphy is only available within a limited interval of the rock column. Usually over all the basins in the world, only a limited part of the sedimentary column in that basin is very well studied and understood so that it can be used as an input to a comprehensive basin simulator with confidence.

(3) The effect of the difference of the dominant frequency between observed and synthetic data.

(4) The influence of missed lithologies in the sediment column used as input for the basin simulator. Any input to a basin modelling effort will always be fraught with uncertainties and missed lithologies.

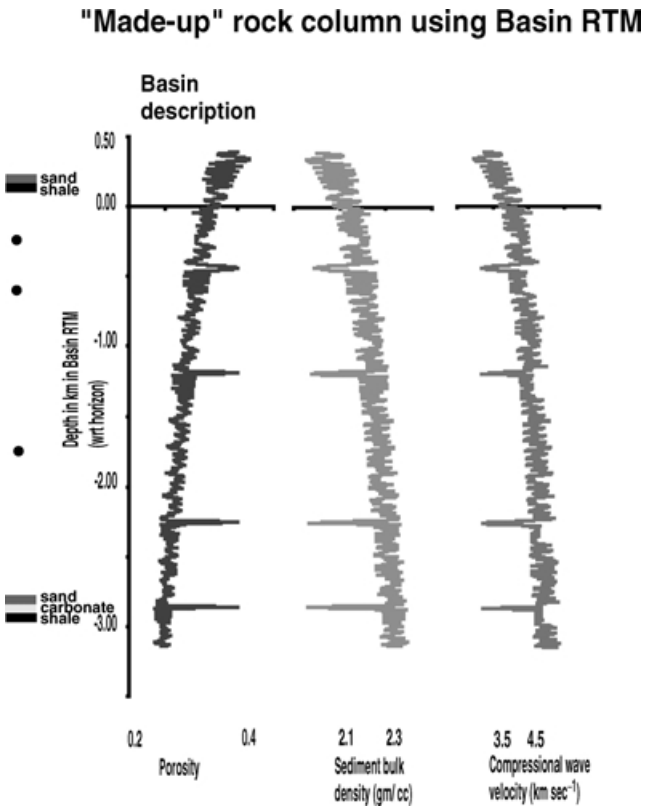

Figure 2. A synthetic profile of porosity, sediment bulk density and *P*-wave velocity generated by a Basin RTM simulation for a geothermal gradient of 30 °C km^{-1} with more than 3 km thick basin interbedded with shales, sandstone and carbonates. These profiles are pseudo-well logs made through complex interaction of various reaction, transport, mechanical processes defined in Section 2 via Basin RTM. The 30 °C km^{-1} simulation is used as 'observed' data for the experiments conducted in this study. The use of parentheses is to distinguish our discussion pertaining to real data sets.

2 APPROACH

2.1 Comprehensive basin modelling

In order to generate the synthetic response, a comprehensive RTM model is required. The advantage of a comprehensive RTM basin model is not only its potential for reliable predictions, but also its ability to predict a fuller suite of the parameters needed to calculate the synthetic response to be compared with a variety of observed data types (for example, seismic and well logs). Predictions include the pressure and composition of the various pore fluid phases; the shape, size, packing and abundance of the minerals; fracture network statistics; and *in situ* stress. These rock and fluid parameters can help one estimate oil and gas reserves in place and the hydrologic and mechanical properties of reservoirs and other sedimentary units. There are two types of quantitative physico-chemical basin models presently in use.

(1) Conventional basin models that have the capability to simulate multiphase flow, but use empirical laws for compaction (Ungerer *et al.* 1990; Forbes *et al.* 1992; Person & Garven 1992; Maubeuge & Lerche 1993, 1994; Bour & Lerche 1994; Luo & Vasseur 1995, 1996; Person *et al.* 1995; Roberts & Nunn 1995; Wieck *et al.* 1995; Yu *et al.* 1995; Gordon & Flemings 1998; Wang & Xie 1998; McPherson & Garven 1999; McPherson & Bredehoeft 2001). Some of these models include petroleum generation (Ungerer *et al.* 1990; Maubeuge & Lerche 1993, 1994; Luo & Vasseur 1996). Fracturing, however, which is an important factor in tight reservoirs, is only considered by a few research groups (Maubeuge & Lerche 1993, 1994; Roberts & Nunn 1995; Wang & Xie 1998; McPherson & Bredehoeft 2001) and is accounted for by assuming that rocks fracture when pore pressure exceeds a certain fraction of the overburden stress. This assumption essentially eliminates the dependence of fracturing on lithologic properties, a fact that is in contradiction to observations from sedimentary basins all over the world. In other approaches, empirical laws are used to relate porosity to effective stress, temperature and other variables to model compaction driven flow in sedimentary basins; this assumption also ignores the dependence of rock properties on lithology.

(2) Basin models with a stress/deformation module (Schneider *et al.* 1996; Luo *et al.* 1998; Suetnova & Vasseur 2000): these models have a better accounting of stress and deformation evolution. However, they ignore multiphase flow and petroleum generation processes that significantly affect the stress and the deformation of a sedimentary basin.

To capture the essence of coupled processes operating in sedimentary basins, a numerical basin model should at least include the following:

(1) A deformation model that accounts for poroelasticity and irreversible deformation mechanisms such as pressure solution and fracturing.
(2) A fracture network dynamics model that is capable of being extended to 3-D.
(3) Rheologic and multiphase parameters co-evolved with diagenesis, compaction and fracturing.
(4) Multiphase flow and petroleum generation.
(5) Inorganic fluid and mineral reactions.
(6) Heat transfer.
(7) Reconstruction of sedimentation/erosion history.

Recently, Tuncay *et al.* (2000a) developed an incremental stress rheology approach for sedimentary basins, which integrates many types of processes that affect rock properties (including, for example, poroelasticity, non-linear viscosity and pressure solution). The statistical treatment of fracture network dynamics provides a significant improvement over existing basin models (Tuncay *et al.* 2000b) as it allows the quantification of anisotropy created dynamically by fracturing and its effects on the total rate of strain and rock mechanical and fluid transport properties. Rocks fracture due to the difference between the fluid pressure and the least compressive stress. However, as fractures open, overall rock volume increases and fluid pressure in the fractures compresses the rock, increasing the compressive stress normal to the fracture plane. Thus, fracturing is a self-limiting process: first, as fractures open, they provide a pathway for fluid escape/depressuring and secondly, the volumetric strain caused by fractures increases the confining stress that reduces the rate of fracture growth. Payne *et al.* (2000) and Tuncay & Ortoleva (2001) have applied this comprehensive approach to the Piceance basin (1-D) and in salt tectonic regimes (2-D).

In this study, we account for fracture network dynamics; incremental stress rheology (with poroelasticity and irreversible temperature-dependent viscous deformation) and single-phase fluid flow for a 1-D approach. The input for Basin RTM is mostly from published literature, public domain data, well logs, etc., and sometimes site specific oil industry propriety data. The input for Basin RTM includes sedimentation composition and grain size, sedimentation/erosion rate, subsidence rate, sea level history, and a

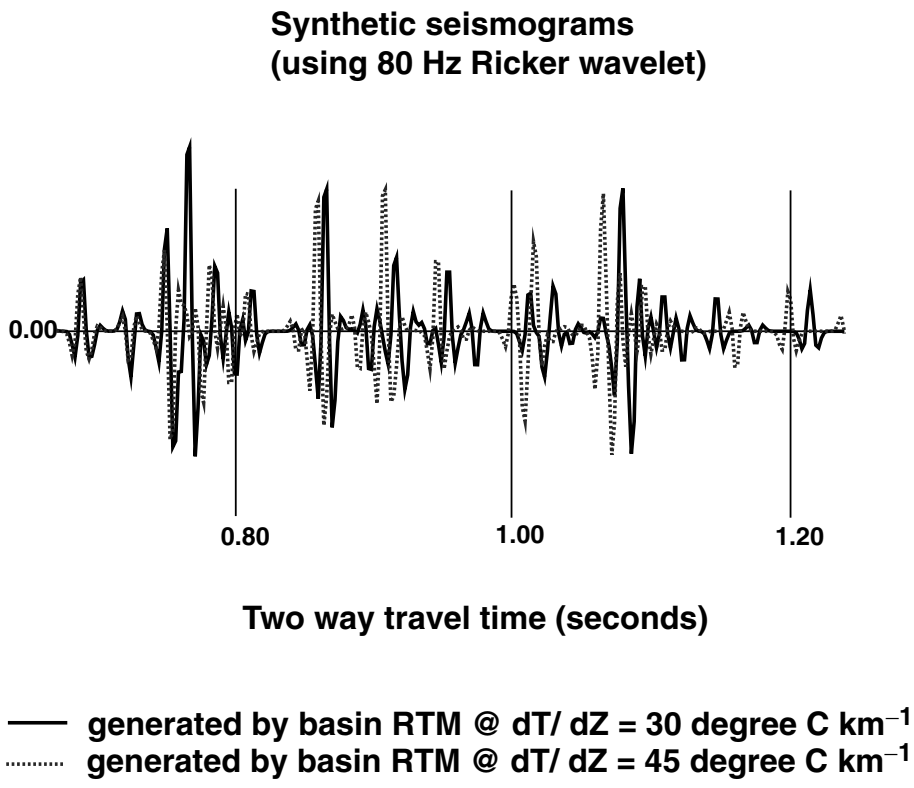

Figure 3. A comparison of synthetic seismograms generated from Basin RTM output at 30 and 45 °C km^{-1} illustrates the strong dependence of the seismic signal on the tectonic history. This interesting observation caused by temperature dependence for fluid and rock properties underlies the viability of the approach suggested in Fig. 1.

number of phenomenological parameters. This all evaluates the rock and fluid transport properties, such as permeability, bulk and shear viscosity (Tuncay et al. 2000a,b, 2001). Basin RTM also has access to thermodynamic and kinetic data for most water–rock interaction phenomena. For example, gamma logs are used to determine the percentage shaliness of a stratigraphic column (Schlumberger Log Interpretation 1972) to be one of the inputs to Basin RTM. We assign a standard mineralogical composition in terms of the percentage of clay minerals, quartz, feldspar, etc. for 100 per cent shales, sandstones and carbonates (Blatt & Traey 1995). Using a percentage shaliness that we calculated from the logs, we calibrate the mineralogical composition accordingly for different rock units when we build our sedimentary basin for numerical simulation.

2.2 Algorithm

Although basin models require a large number of phenomenological parameters and geologic boundary conditions, only a few studies have focused on the utilization of observed data to constrain the model (Lerche 1991; Maubeuge & Lerche 1993; Zhao & Lerche 1993; Yu *et al.* 1995). Uncertainty in basin modelling is reviewed in detail by Tuncay & Ortoleva (2003). Here we concentrate on data/model integration to determine tectonic parameters, notably the temperature gradient, using reflection seismic data.

Our approach for automatically estimating the geothermal gradient based on our seismic inversion-basin modelling algorithm is as follows. Fig. 1, (1) an optimization technique (iterative quadratic fitting or simulated annealing) is used to select a geothermal gradient for a Basin RTM simulation. (2) Using this geothermal gradient, the basin simulator predicts the present-day rock and fluid properties. (3) Predicted rock and fluid properties are used to construct sediment bulk density and *P*-wave velocity profiles (Fig. 2), (4) a synthetic seismogram is generated from the calculated properties (Fig. 3), (5) the error between the synthetic and observed seismograms is computed and used to guide the search for the error-minimizing geothermal gradient in an iterative fashion.

2.3 Synthetic seismograms

A linear convolution approach was implemented for computing the synthetic seismograms (Peterson *et al.* 1955). The reflection coefficients were calculated from the Basin RTM output and convolved with a source wavelet to produce the synthetic seismogram. The linear convolution approach does not take into account the effects of internal multiples, attenuation or spherical divergence. *P*-wave velocity depends on pore pressure, grain size, porosity, rock composition, fracture statistics, etc. (Murphy 1982; Klimentos & McCann 1983; Nagano 1998). In this study, *P*-wave velocity was calculated as a function of the porosity and texture of the unfractured rock using the approach of Berryman (1986). Fig. 3 shows a comparison of two synthetic seismograms obtained for different geothermal gradients. In this particular example, higher geothermal gradient results in a more compact rock column as a result of higher rate of compaction. However, one should be cautious in generalizing this result. Higher temperatures can also increase fluid pressure to lithostatic levels and can retard/stop compaction as effective stress becomes small. Furthermore, as mineral composition of a sedimentary layer varies, compaction rates do not increase uniformly throughout the basin.

2.4 Error measures

Various measures of the error between the observed and synthetic seismograms were used to evaluate their suitability for our

algorithm. Measures for the error in the time-series x_i (observed) and y_i (synthetic) are as follows.

Our definition for linear correlation is the same as Pearson's linear correlation coefficient, r (Press *et al.* 1993), except for a minus sign:

$$r = -\frac{\sum_{i=1}^{N}(x_i - \bar{x})(y_i - \bar{y})}{\sqrt{\sum_{i=1}^{N}(x_i - \bar{x})^2}\sqrt{\sum_{i=1}^{N}(y_i - \bar{y})^2}},$$

where $\bar{x} = \frac{1}{N}\sum_{j=1}^{N} x_j$ and similarly for $\bar{y}$. A minus sign is incorporated so that a minimum in the error occurs at the observed geothermal gradient. According to the above formulation, a 'perfect correlation' between two time-series is -1. If the values of r are close to zero, then the two time-series x_i and y_i are uncorrelated. Alternatively, power spectra for the time-series x_i and y_i can be used to quantify error.

The mean square error e for time-series x_i and y_i is defined via

$$e = \sum_{i=1}^{N}(x_i - y_i)^2.$$

The mean square error e_{na} based on next same arrival time is defined via

$$e_{\mathrm{na}} = \sum_{i=2}^{N}\left(t_i^x - t_i^y\right)^2,$$

where $t_i^x = x_i - x_{i-1}$ and similarly for $t^y{}_i$.

2.5 Optimization techniques

We experimented with two optimization techniques (iterative quadratic fit and simulated annealing) for finding the global minimum of the various error measures. A critique of Monte Carlo, simulated annealing, and genetic algorithms as applied to minimization methods in geophysics is presented in Sen & Stoffa (1995). As greedy algorithms, such as simulated annealing require many iterations and as each iteration requires a computationally expensive basin simulation in the present context, one expects that they would not be practical. In the iterative quadratic fit method, we fit the error to a quadratic function based on simulations for three geothermal gradients (or 3^d simulations when the number of tectonic parameters to be estimated is d). Using the coefficients from the curve fit, the geothermal gradient that minimizes the error is computed. The location of this minimum is then used as the centre point for the next quadratic fitting cycle to refine the location of the minimum. This cycle is repeated until the error difference between the minima from most recent and previous iteration is less than a specified tolerance. The weakness of this method is that it may only find a local, and not a global, minimum.

Simulated annealing is a minimization algorithm capable of finding a global minimum despite the presence of local minima (Otten & van Ginneken 1989; Sen & Stoffa 1995). The simulated annealing technique implemented here is based on the Cauchy cooling algorithm (Szu & Hartley 1987, Taygeta Scientific Inc.). The Cauchy cooling algorithm is a fast annealing technique compared to the other Boltzmann algorithms (Ingber 1993). Rothman (1985, 1986), Basu & Frazer (1990) and Sen & Stoffa (1991) have used simulated annealing in geophysical applications. The simulated annealing approach is quite analogous to the manner in which liquids freeze or metals crystallize during annealing (Kirkpatrick *et al.* 1983). The simulated annealing search initially is very disorderly similar to the thermodynamic state of the melt at high temperatures (Kirkpatrick *et al.* 1983). Such an approach enables one to span the entire error space and not be stuck in local minima during optimization. As error minimization continues, the approach becomes more orderly and enables one to find a global minimum in a similar fashion as a system in nature achieves thermodynamic equilibrium when cooled slowly (Kirkpatrick *et al.* 1983). The algorithm is set up in terms of a thermodynamic system described in terms of temperature, energy, and with the probability of accepting a change in energy given through Boltzmann factor (Kirkpatrick *et al.* 1983). Our experience showed that the performance of simulated annealing optimatization technique depended on the rate with which the system was cooled, meaning thereby how quickly we proceeded in our choice of geothermal gradients (coarser sampling of the error space) toward the global minimum. A slow cooling approach was expensive but was much more robust in finding a global minimum compared with a faster approach. The strength of simulated annealing is that the algorithm is capable of determining a global minimum even when the error function is very rugged in shape, full of local minima. However, the drawback of the simulated annealing algorithm is that it is a greedy algorithm and quite time-consuming computationally.

3 NUMERICAL EXPERIMENTS

Numerical experiments are carried out using a Basin RTM simulation run with a geothermal gradient of 30 °C km^{-1} to generate the 'observed' seismic data. As the present study concentrates on the development and the robustness of the technique, we used a seismogram from a 30 °C km^{-1} basin simulation as a proxy for 'observed' data rather than using actual reflection seismic data. In an approach such as this, an actual reflection seismic data will be a single trace taken from a multichannel, stacked, migrated, reflection seismic section intersecting a well or borehole location, as used in many standard seismogram modelling approaches (Lorenzo & Hesselbo 1996; Tandon *et al.* 1998).

For our study, we built a 3.5 km sedimentary basin that is a composite made from data originally from Piceance and East Texas basins. The results of Fig. 2 are generated from a 112 myr simulation of a 3.5 km (present-day) stratigraphic column with interbedded sand, shale and carbonate lithologies. The 'observed' rock record consists of 225 layers, with thicknesses varying from 5 to 15 m. The corresponding seismogram and the associated data used in Basin RTM from 30 °C km^{-1} simulation is the 'observed' data for our set of experiments. Different levels of random noise are added to this 'observed' seismogram (see the Appendix). Seismograms from Basin RTM simulations at different geothermal gradients are part of the inversion technique (Fig. 1) to figure out the correct geothermal gradient via error minimization.

We assume that the 'observed' seismic reflection data contains ambient noise that is coloured in nature (Ursin *et al.* 1996). The majority of the noise in an observed data is removed via higher-fold stacking, f-k, and coherent filtering (Yilmaz 1987). Frequency content of ambient noise typical in seismic reflection data can be both low (0–2 Hz) and high (16–32 Hz) (Larner *et al.* 1983; Yilmaz 1987). However, in general, most noise in the stacked seismic data is source generated and scattered surface waves which dominantly have lower frequency content (Larry Brown, personal communication). The effect of incoherent noise is ignored since they are quite low in amplitude (Sheriff & Geldart 1995).

Experimental studies in source-generated noise identify a frequency bandwidth of 2–12 Hz for noise analysis (Jolly & Mifsud 1971). Similarly, experiments on surface waves display a 0.2–5 Hz bandwidth (Douze 1964). A seismic noise experiment at Roosevelt Hot Springs showed a bandwidth of 0.5–10 Hz and frequencies

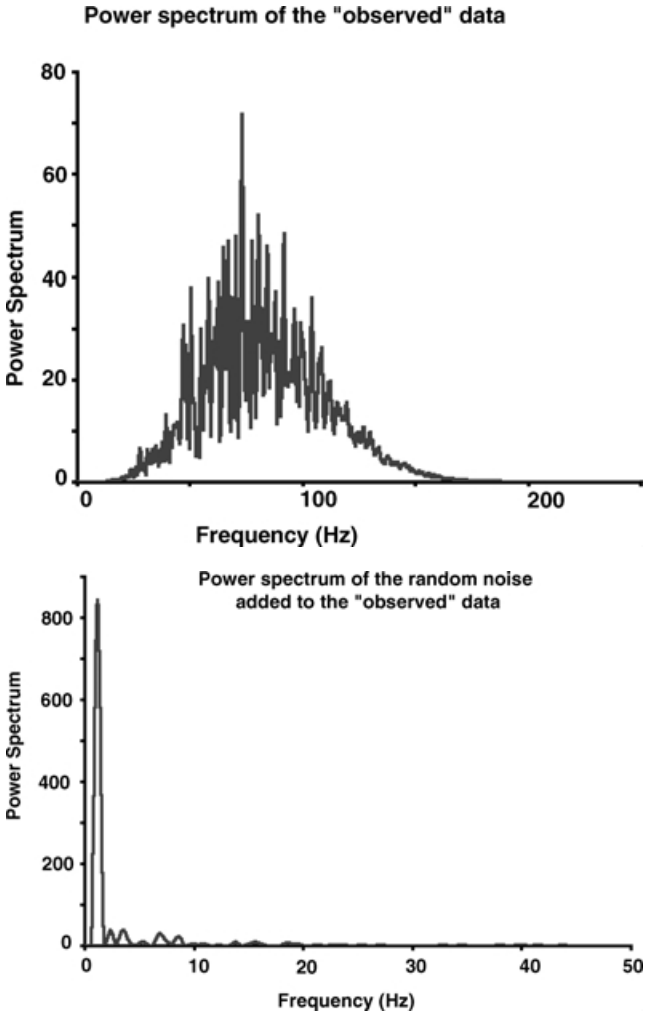

Figure 4. (a) A power spectrum of the 'observed' noise-free seismic data (Fig. 3). (b) A power spectrum of the noise added to the 'observed' data. The figure shows the noise at 50 per cent level and its dominantly low frequency content to simulate typical noise that could be present in a stacked seismic reflection data even after seismic data processing (Yilmaz 1987).

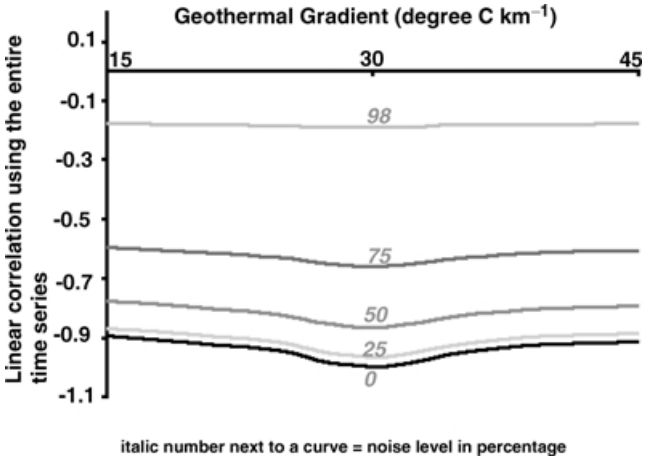

Figure 5. The variation of linear correlation error to be part of the seismic inversion-basin modelling scheme (Fig. 1) at different noise levels using the entire time-series.

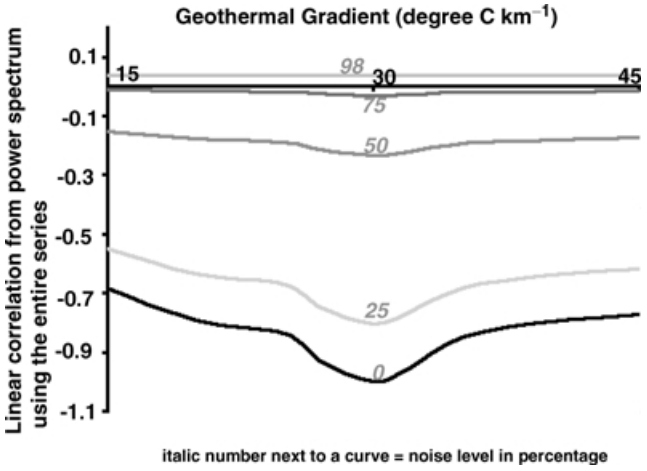

Figure 6. A linear correlation error based on the power spectrum of the seismograms to be part of the seismic inversion-basin modelling scheme (Fig. 1) at different noise levels.

>10 Hz displayed no spatial coherence (Douze & Laster 1979). Therefore, in this study the bandwidth for the random noise that is added to the 'observed' data is 0.6–20 Hz. The contribution from higher frequencies is generally considered unimportant for a stacked trace and was thus neglected (Fig. 4b). The frequency bandwidth of the 'observed' data (Fig. 4a) is much wider than that of the noise.

Experiment 1: choice of best error measure

Numerical experiments (Figs 5–7) show that linear correlation and quadratic error yield a single minimum in the error over the range of geothermal gradient values (15–45 °C km^{-1}) typically found in sedimentary basins (Turcotte & Schubert 1982). This character persists in the presence of noisy 'observed' data (Figs 5–7). The linear correlation error both using the time-series and their power spectra displays a global minimum even when the noise level in the 'observed' data is 75 per cent (Figs 5 and 6). If in the real reflection seismic data, higher-frequency noise was present then the global minimum will not be observable at 75 per cent noise level. In the quadratic error, the global minimum is not well defined since the presence of random noise flattens the error function at lower levels than for linear correlation (Fig. 7). This implies the effect of attenuation and geometric spreading in the observed seismic data can make any error measure based on mean square amplitude difference unreliable. Fig. 8 shows that the quadratic error based on next arrival time does not display the global minimum at noise levels as low as 25 per cent. We conclude that linear correlation error using time-series or power spectra was found to be the most effective measure for our methodology.

Experiment 2: model data with detailed stratigraphic layering in a limited depth interval

When using real basin data, it is very unlikely that one would have detailed information on lithologies over the entire stratigraphic column that can be used as input data in a comprehensive basin simulator and perform seismic inversion. We think this is an important experiment to test the feasibility of such an approach, as the entire stratigraphic column in any basin around the world is not very well understood and studied. To study the effects of the lack of stratigraphic data in the shallower depths, the first second out of 1.742 s two-way traveltime is truncated in the synthetic seismograms. With this truncation, only the last 42 per cent of the

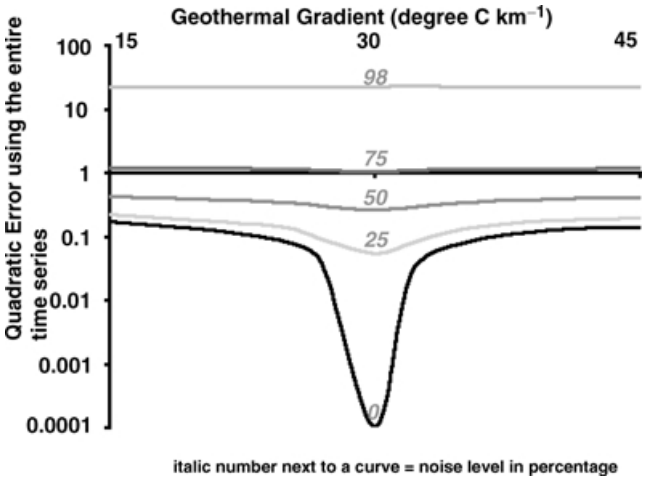

Figure 7. The variation of quadratic error based on the power spectrum of the seismograms to be part of the seismic inversion-basin modelling scheme (Fig. 1) at different noise levels. The error function is truncated to 0.0001 to avoid minus infinity in the noise-free graph.

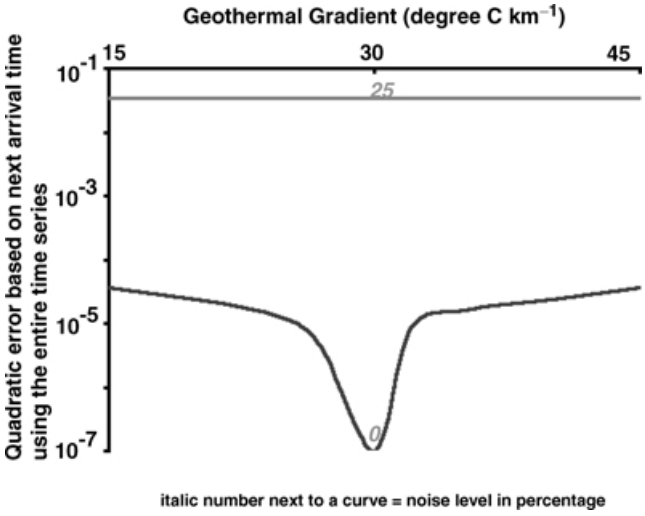

Figure 8. The variation of quadratic error based on the next arrival time using the entire time-series to be part of the seismic inversion-basin modelling scheme (Fig. 1). The error function is truncated to 10^{-7} to avoid minus infinity in the noise-free graph.

synthetic seismograms from our inversion is representative of the 'observed' one to even perform error analysis. An example of detailed data sets could be reservoirs from well developed oil and gas fields, e.g. those in Gulf of Mexico or North Sea. These will have enough wealth of data to explore the complex interaction of physics and chemistry of the sedimentary basins and perform inversion (Fig. 1). The physical and chemical processes are affected most strongly by the geothermal gradient in the deeper parts of the basin. Thus one might expect that a selected time interval from the deeper parts of the basin would be sufficient to determine a tectonic parameter, such as geothermal gradient. Fig. 9 shows that one can find a global minimum even in the presence of noise at 75 per cent level. If the linear correlation error uses the entire time-series, even if the Basin RTM simulation is coarser in certain intervals, then the global minimum value is lower. Experiments 3 and 4 are also performed using only partial time-series (from 1.0 to 1.742 s two-way traveltime).

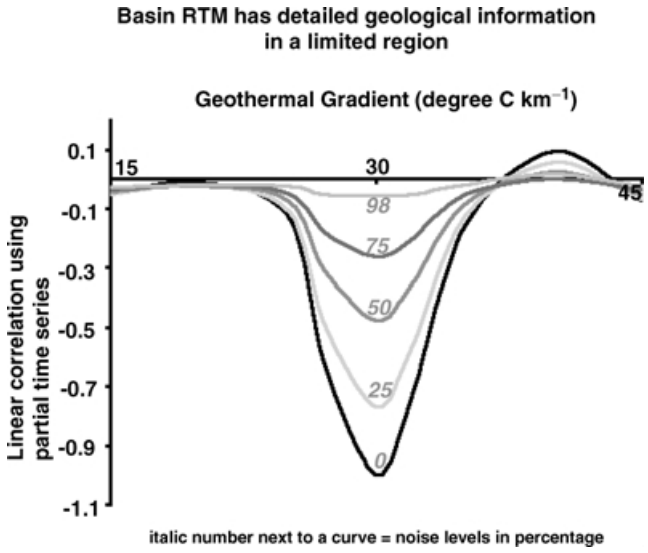

Figure 9. A linear correlation error when the first second of the 'observed' seismogram is not used in the error calculation. This is to highlight that error analysis is being done in a limited part, as there might not be enough detailed data for the shallower section of the sedimentary basin.

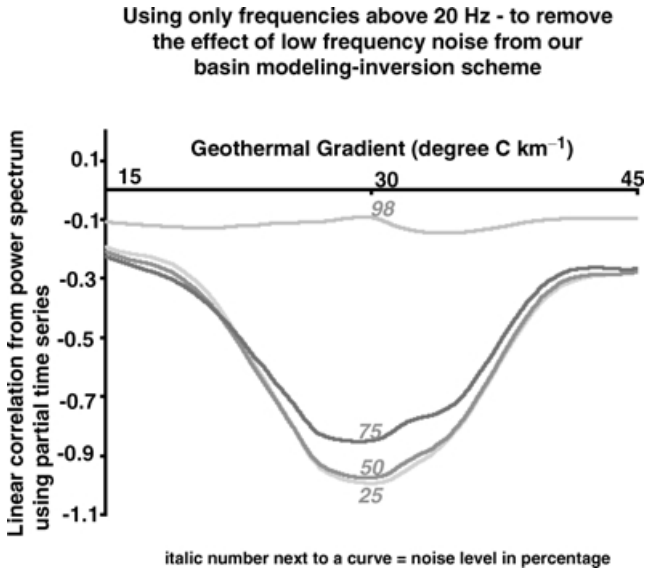

Figure 10. A linear correlation error based on the power spectrum using frequencies above 20 Hz and partial time-series. Error analysis in a limited frequency bandwidth can always be used to exclude noisy part of the data in the power spectrum.

As the noise level increases, the global minimum becomes shallower if linear correlation error is used (Fig. 9). In the case demonstrated here, the majority of noise added to the 'observed' data is less than 20 Hz (Fig. 4). If the linear correlation error is calculated using power spectra with only frequencies above 20 Hz, then the algorithm yields a deeper global minimum even in the presence of appreciable noise (Fig. 10). Therefore, using power spectra for error analysis within a selective frequency bandwidth seems to enhance the results of our approach. Excluding frequencies from error analysis is beneficial only if the stacked noise has distinctly different frequency content than does the frequency bandwidth from the majority of the reflectors. Noise analysis is always carried out in seismic surveys that will enable us to determine power spectra of the noise and help

in our technique when implemented on real data. When the power spectra of the noise and data are not clearly distinct (Fig. 4), then the linear correlation error using time-series (Fig. 5) along with power spectra (Fig. 6) should be used with care.

In real sedimentary basin examples, one can also use the existing the biostratigraphic information to calibrate the top horizon between the real seismogram data and modelled synthetic seismograms for the limited stratigraphic column that is being used in our inversion technique via time correction (Tandon *et al.* 1998) (Fig. 1). A time correction can also be used to correct for mismatch that might be caused by missing details from a shallower part of the basin as an input to the basin simulator.

Experiment 3: observations and synthetic seismograms with different frequencies

Attenuation and spherical divergence cause a loss of higher frequencies in the seismic reflection data. Attenuation and spherical divergence were not incorporated in the generation of synthetic seismograms used in this study. Even if these effects were included, it is likely that there always will be some difference in frequency content between the observed and synthetic data. To investigate these effects, the 'observed' and synthetic seismograms are constructed using 40 and 80 Hz Ricker wavelets, respectively. A 40 Hz difference between the 'observed' and synthetic seismograms approximates the loss of higher frequencies in a sedimentary basin due to attenuation and spherical divergence in the observed data. Fig. 11 shows that one can still find the global minimum at 75 per cent noise levels. Note that a 80 Hz Ricker wavelet is used for both 'observed' and synthetic seismograms in experiments 1, 2 and 4.

The range of frequencies for exploration seismology is generally 2–120 Hz (Sheriff & Geldart 1995). Use of an 80 Hz Ricker wavelet constitutes a high-resolution, basin scale reflection seismic reflection survey. In shallow seismic reflection exploration (100–200 m), the dominant frequency can be as high as 1000 Hz (Buhnemann & Holliger 1998), but we are more concerned in surveys that image even the deeper parts of the basin. A 40 Hz Ricker wavelet for the 'observed' data is chosen to mimic the effect of attenuation on the dominant frequency content. Typically, dominant frequencies observed in reflection seismic data lie between 5–50 Hz (Sheriff & Geldart 1995).

Experiment 4: basin data with missing lithologies

In this section, we investigate the effects of resolution in the basin model and observed seismic reflection data. In general, resolution of the seismic reflection data is 1/4–1/8 of the dominant wavelength of the source wavelet (Sheriff 1977). Deviations in the description of layering in the model on a similar or higher scale are expected to affect the algorithm. The purpose of this experiment is to determine whether the algorithm fails when the model response does not correspond exactly to the layering of the stratigraphic column sampled by the mechanical waves as in the 'observed' seismic data. It is unlikely that the sediment density and *P*-wave profiles from the basin simulator exactly correspond to the layering of the actual rock. Most likely, the basin model will not be able to simulate all the heterogeneities sampled by the seismic waves in a controlled source experiment.

To generate an incomplete basin model input, we removed every eighth layer from the entire model input data and the thickness of the seventh layer was increased to compensate for the removed layer. Such missing layers not only result in the absence of reflectors in the synthetic seismogram, but also lead to a perturbed velocity/depth curve. It was found that a global minimum can be determined using linear correlation error based on power spectra (with only frequencies above 20 Hz) in the presence of 75 per cent noise level (Fig. 12).

In a similar experiment, every fourth layer from the basin input was removed from the basin input data. Fig. 13 shows that the correct global minimum can approximately be determined using the linear correlation error of power spectra (frequencies above 20 Hz). Therefore, the layering, the bulk density, and *P*-wave velocity profiles generated by Basin RTM need not be perfectly matched even in a limited stratigraphic column for our algorithm to work.

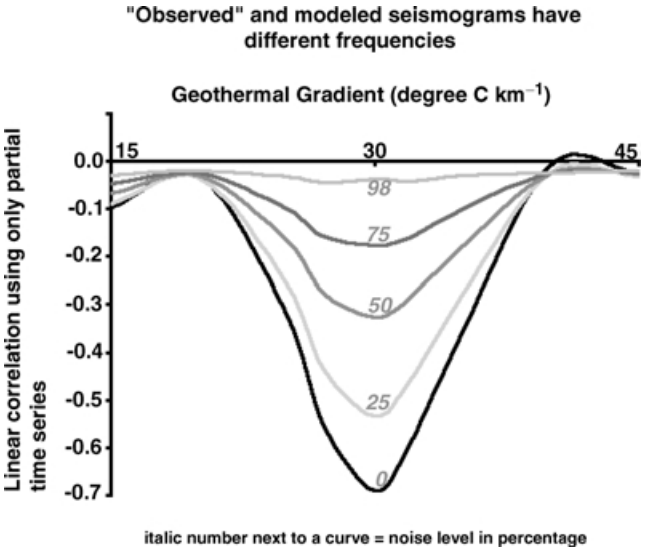

Figure 11. A linear correlation error based on the partial time-series. The 'observed' and synthetic seismograms are calculated using 40 and 80 Hz Ricker wavelets, respectively, to demonstrate the effect of attenuation.

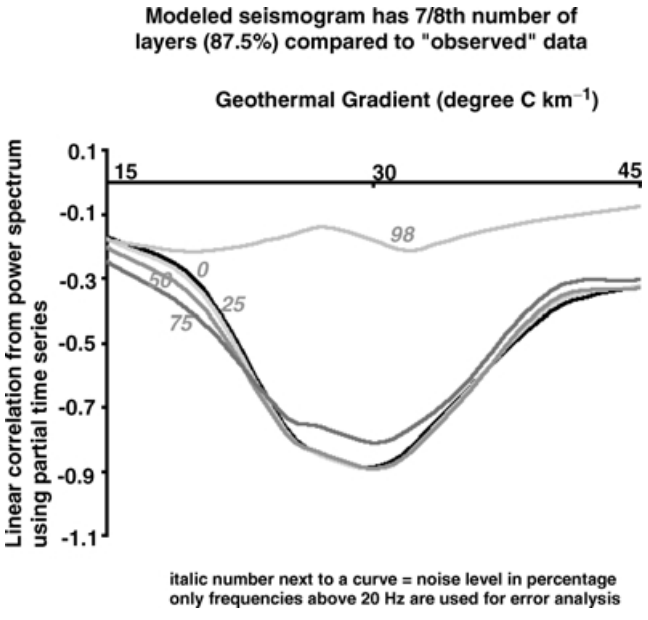

Figure 12. A linear correlation error based on the power spectrum using the partial time-series and frequencies above 20 Hz. Every eighth lithologic layer was missed in the basin simulator input to test the robustness of the procedure to insufficient lithologic delineation.

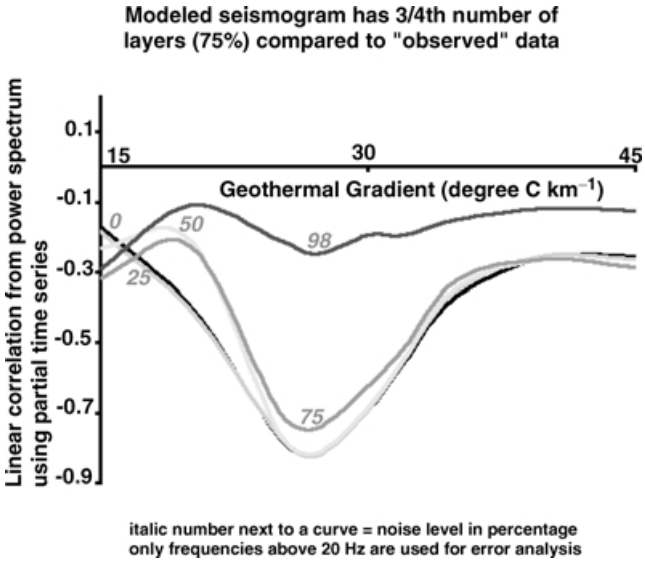

Figure 13. The same as Fig. 12 except that every fourth layer was missed in the basin simulator input.

4 CONCLUSIONS

The basin simulation-enhanced seismic inversion method has been shown to be a viable approach to delineating the state of the subsurface and the heterogeneities formed in the sedimentary basin. The method has the potential for greatly reducing the cost and accuracy of seismic exploration and understanding of the rheological evolution of sedimentary basins in response to varying tectonic parameters. However, the present study has even wider implications. We suggest that it provides an approach for integrating many types of basin data (well logs, geochemical, core analysis and thermal data) in addition to seismic data to yield one integrated approach by generalizing the algorithm of Fig. 1. Thereby, basin modelling enhances the quality of data analysis and enhances the results of basin simulation all in one unified, automatable and parallelizable computational approach for data assimilation.

The present study is only preliminary and presents a new methodology being developed. This study lays down the theoretical framework for future work where basin modelling and multiple data sets are fully integrated. Further studies will include actual examples from sedimentary basins in different parts of the world. The basin simulation was carried out in one, and not three, spatial dimensions—limiting the level of reliability. The basin model used, Basin RTM, while arguably the most comprehensive model available at this writing, still could benefit from the addition of other processes and the refinement of its rheological, hydrologic, and reaction rate laws. Furthermore, limitations due to the intensive computational demands of our procedure will place some restrictions on its widespread use for the next several years. However, this is a first step in understanding a detailed, complex evolution of heterogeneities in sedimentary basins that are capable of being imaged by reflection seismic data and can be used for geoinfomatics of sedimentary basins.

Another concern that should be addressed in future research pertaining to our method or similar methods is the uniqueness of the inversion/prediction. Can there be other geothermal histories that give the same seismic data? Also, do the predictions reflect the true content of the data or is the latter masked by an incomplete model or one based on an erroneous rheological or other rate laws? One must also remember that even the most comprehensive model is never a complete description of the complexity that is present in a sedimentary basin. Finally, methods that simultaneously provide an estimate of uncertainty in the inversion and risk in the strategy based on the predictions should be used (Tuncay & Ortoleva 2003).

Our algorithm works even when the model has a detailed stratigraphic description in a limited region with incomplete stratigraphic data (12.5–25 per cent absent). As a result of the shape of the geothermal gradient-linear correlation error measure, the iterative quadratic fitting is a more efficient optimization technique than simulated annealing. Of all the error measures used, linear correlation error of the power spectrum between the observed and synthetic seismograms is the most ideal choice. If the power spectrum of noise and dominant reflectivity in the observed data are different, then the error analysis in a selected frequency bandwidth makes our algorithm even more robust.

Our methodology is viable even (1) in the presence of large amounts of low-frequency noise in the seismic data, (2) when information concerning detailed stratigraphic layering is confined to a limited region and (3) frequency content of the observed and predicted seismograms differ. The necessary requirement for the methodology to succeed is the availability of detailed geological information in a sedimentary basin. In earth sciences, the maximum wealth of geological, geochemical and geophysical data for sedimentary basins has been collected by academic, oil and gas, mining industry endeavours for centuries. Therefore, approaches that attempt to put all these data sets together in a rigorous fashion and their potential for prediction should be fully explored.

ACKNOWLEDGMENTS

This work was supported by the National Energy Technology Laboratory (NETL) of the US Department of Energy through contract no. DE-AC26-00NT40689. We thank Dr Frances Toro (NETL) for her constructive critiques and encouragements. We thank Dr Juan Lorenzo (Louisiana State University) for providing us with his synthetic seismogram programme and Dr Everett Carter (Taygeta Scientific Inc., www.taygeta.com) for the use of the simulated annealing code. Power spectra was calculated using FFTW, a *C* subroutine library for computing discrete Fourier transforms (www.fftw.org). Support from Publications and Outreach office at COAS to KT is highly appreciated. Comments from an anonymous reviewer and the Associate Editor, Steven Ward are greatly appreciated as they improved the manuscript.

REFERENCES

Basu, A. & Frazer, L.N., 1990. Rapid determination of critical temperature in simulated annealing inversion, *Science,* **249,** 1409–1412.

Berryman, J.G., 1986. Effective medium approximation for elastic constants of porous solids with microscopic heterogeneity, *J. appl. Phys.,* **59,** 1136–1140.

Blatt, H. & Tracey, R., 1995. *Petrology, Igneous, Sedimentary and Metamorphic,* W.H. Freeman & Co.

Boadu, F.K., 1998. Inversion of fracture density from seismic velocities using artificial neural networks, *Geophysics,* **63,** 534–545.

Bour, O. & Lerche, I., 1994. Numerical modelling of abnormal fluid pressures in the Navarin Basin, Bering Sea, *Marine and Petroleum Geology,* **11,** 491–500.

Buhnemann, J. & Holliger, K., 1998. Comparison of high-frequency seismic sources at the Grimsel test site, central Alps, Switzerland, *Geophysics*, **63,** 1363–1370.

Cabrera, G.R., 1996. Application of geostatistical techniques to 3-D, 3-C seismic and core studies to estimate reservoir porosity in the lower Nisku

interval at Joffre Field, Alberta, Canada, *Master's thesis,* Colorado School of Mines, Colorado.

Douze, E.J., 1964. Signal and noise in deep wells, *Geophysics*, **29,** 721–732.

Douze, E.J. & Laster, S.J., 1979. Seismic array noise studies at Roosevelt Hot Springs, Utah geothermal area, *Geophysics*, **44,** 1570–1583.

Forbes, P.L., Ungerer P. & Mudford, B.S., 1992. A two dimensional model of overpressure development and gas accumulation in Venture Field, Eastern Canada, *AAPG Bulletin,* **76,** 318–338.

Gordon, D.S. & Flemings, P.B., 1998. Generation of overpressure and compaction-driven fluid flow in a Plio-Pleistocene growth-faulted basin, Eugene Island 330, offshore Louisiana, *Basin Research,* **10,** 177–196.

Ingber, A.L., 1993. Simulated annealing: Practice versus theory, *J. Mathl. Comput. Modeling,* **18,** 29–57.

Jolly, R.N. & Mifsud, J.F., 1971. Experimental studies of source-generated seismic noise, *Geophysics*, **36,** 1138–1149.

Kirkpatrick, S., Gelatt, C.D., Jr & Vecchi, M.P., 1983. Optimization by simulated annealing, *Science,* **220,** 671–680.

Klimentos, T. & McCann, C., 1983. Relationships among compressional wave attenuation, porosity, clay content, and permeability in sandstones, *Geophysics*, **55,** 998–1014.

Larner, K., Chambers, R., Yang, M., Lynn, W. & Wai, W., 1983. Coherent noise in marine seismic data, *Geophysics*, **48,** 854–886.

Lerche, I., 1991. Inversion of dynamical indicators in quantitative basin analysis models. I. Theoretical considerations, *Mathematical Geology,* **23,** 817–832.

Lorenzo, J.M. & Hesselbo, S., 1996. Seismic-to-well correlation at ODP 150 continental slope sites, *Proc. Ocean Drilling Program, Scientific Results,* **150,** 293–307

Luo, X. & Vasseur, G., 1995. Modelling of pore pressure evolution associated with sedimentation and uplift in sedimentary basins, *Basin Research,* **7,** 35–52.

Luo, X. & Vasseur, G., 1996. Geopressuring mechanism of organic matter cracking: numerical modeling, *AAPG Bulletin,* **80,** 856–873.

Luo, X., Vasseur, G., Pouya, A., Lamoureux-Var, V. & Poliakov, A., 1998. Elastoplastic deformation of porous medium applied to the modeling of compaction at basin scale, *Marine and Petroleum Geology,* **15,** 145–162.

McPherson, B.J.O.L. & Bredehoeft, J.D., 2001. Overpressures in the Uinta Basin, Utah: Analysis using a three-dimensional basin evolution model, *Water Resources Research,* **37,** 857–871.

McPherson, B.J.O.L. & Garven, G., 1999. Hydrodynamics and overpressure mechanisms in the Sacramento Basin, California, *Am. J. Sci.,* **299,** 429–466.

McQuillin, R., Bacon, M., & Barclay, W., 1984. *An introduction to seismic interpretation: reflection seismics in petroleum exploration,* Graham and Trotman, London.

Mallick, S., Craft, K.L., Meister, L.J. & Chambers, R.E., 1998. Determination of the principal directions of azimuthal anisotropy from P-wave seismic data, *Geophysics*, **63,** 692–706.

Maubeuge, F. & Lerche, I., 1993. A north Indonesian basin: Geothermal and hydrocarbon generation histories, *Marine and Petroleum Geology,* **10,** 231–245.

Maubeuge, F. & Lerche, I., 1994. Geopressure evolution and hydrocarbon generation in a north Indonesian basin: two-dimensional quantitative modeling, *Marine and Petroleum Geology,* **104,** 104–115.

Murphy, W.F., 1982. Effects of partial water saturation on attenuation in Massilon sandstone and Vycor porous glass, *J. acoust. Soc. Am.,* **71,** 1458–1468.

Nagano, K., 1998. Crack-wave dispersion at a fluid-filled fracture with low-velocity layers, *Geophys. J. Int.,* **134,** 903–910.

Otten, R.H.J.M. & van Ginneken, L.P.P.P., 1989. *The Annealing Algorithm,* Kluwer Academic Publishers.

Payne, D.F., Tuncay, K., Park, A., Comer, J. & Ortoleva, P., 2000. A reaction-transport-mechanical approach to modelling the interrelationships between gas generation, overpressuring, and fracturing—Implications for the Upper Cretaceous natural gas reservoirs of the Piceance Basin, Colorado, *AAPG Bulletin,* **84,** 545–565.

Person, M. & Garven, G., 1992. Hydrologic constraints on petroleum generation within continental rift basins: Theory and application to the Rhine Graben, *AAPG Bulletin,* **76,** 468–488.

Person, M., Toupin, D. & Eadington, P., 1995. One-dimensional models of groundwater flow, sediment thermal history and petroleum generation within continental rift basins, *Basin Research,* **7,** 81–96.

Peterson, R.A., Fillipone, W.R. & Coker, E.B., 1955. The synthesis of seismograms from well log data, *Geophysics*, **20,** 516–538.

Press, W.H., Teukolsky, S.A., & Vetterling, W.T., 1993. *Numerical recipes in C: The art of scientific computing,* Cambridge University Press, Cambridge.

Ramos, A.C.B. & Davis, T.L., 1997. 3-D AVO analysis and modeling applied to fracture detection in coalbed methane reservoirs, *Geophysics*, **62,** 1683–1695.

Roberts, S.J. & Nunn, J.A., 1995. Episodic fluid expulsion from geopressured sediments, *Marine and Petroleum Geology,* **12,** 195–204.

Rothman, D.H., 1985. Nonlinear inversion, statistical mechanics, and residual statics estimation, *Geophysics*, **50,** 2784–2796.

Rothman, D.H., 1986. Automatic estimation of large residual statics correction, *Geophysics*, **51,** 337–346.

Schlumberger Log Interpretation, 1972. *Principles/Applications*, Schlumberger Educational Services.

Schneider, F., Potdevin, J.L., Wolf, S. & Faille, I., 1996. Mechanical and chemical compaction model for sedimentary basin simulators, *Tectonophysics*, **263,** 307–317.

Sen, M.K. & Stoffa, P.L., 1991. Nonlinear one-dimensional seismic waveform inversion using simulated annealing, *Geophysics*, **56,** 1624–1638.

Sen, M.K. & Stoffa, P.L., 1995. Global optimization methods in geophysical inversion, in *Advances in Exploration Geophysics 4,* ed. Berkhout, A.J., Elsevier.

Sheriff, R.E., 1977. Limitations on resolution of seismic reflections and geologic detail derivable from them. in *Seismic Stratigraphy—Applications to Hydrocarbon Exploration,* Vol. 26, pp. 3–14, ed. Payton, C.E., Am. Assoc. Pet. Geol. Mem.

Sheriff, R.E. & Geldart, L.P., 1995. *Exploration Seismology,* Cambridge University Press.

Suetnova, E. & Vasseur, G., 2000. 1-D modelling rock compaction in sedimentary basins using a visco-elastic rheology, *Earth planet. Sci. Lett.*, **178,** 373–383.

Szu, H. & Hartley, R., 1987. Fast simulated annealing, *Physics Letters A,* **122,** 157–162.

Tandon, K., Lorenzo, J.M. & de la Linde Rubio, J., 1998. Timing of rifting in the Alboran Sea Basin—Correlation of borehole (ODP Leg 161 and Andalucia A-1) to seismic reflection data: implications for basin formation, *Marine Geology,* **144,** 275–294

Tuncay, K. & Ortoleva, P., 2001. Salt tectonics as a self-organizing process: a three dimensional reaction, transport and mechanics model, *J. geophys. Res.*, **106,** 803–818.

Tuncay, K. & Ortoleva, P., 2003. Quantitative basin modeling: Present state and future developments towards predictibility, *Geofluids,* in press.

Tuncay, K., Park, A. & Ortoleva, P., 2000a. Sedimentary basin deformation: An incremental stress approach, *Tectonophysics*, **23,** 77–104.

Tuncay, K., Park, A. & Ortoleva, P., 2000b. A forward fracture model to predict fracture orientation and properties, *J. geophys. Res.*, **105,** 16 719–16 735.

Turcotte, D.L. & Schubert, G., 1982. *Geodynamics: Applications of Continuum Physics to Geological Problems,* John Wiley & Sons.

Ungerer, P., Burrus, J., Doligez, B., Chenet, P.Y. & Bessis, F., 1990. Basin evaluation by integrated two-dimensional modeling of heat transfer, fluid flow, hydrocarbon generation, and migration, *AAPG Bulletin,* **74,** 309–335.

Ursin, B., de Matos Neto, J.B. & Posani, M.J., 1996. Seismic reflection estimation with colored noise, *Journal of Seismic Exploration,* **5,** 51–62.

Yilmaz, O., 1987. *Seismic Data Processing, Investigations in Geophysics,* Vol. 2, ed. Doherty, S.M., Society of Exploration Geophysicists.

Yu, Z., Lerche, I. & Bour, Q., 1995. Inversion of dynamical indicators in quantitative basin analysis models. III. Multiwell information and two-dimensional case histories, *Mathematical Geology,* **27,** 41–68.

Wang, C. & Xie, X., 1998. Hydrofracturing and episodic fluid flow in shale-rich basins—A numerical study, *AAPG Bulletin,* **82,** 1857–1869.

Wieck, J., Person, M. & Strayer, L., 1995. A finite element method for simulating fault block motion and hydrothermal fluid flow within rifting basins, *Water Resources Research,* **31,** 3241–3258.

Zhao, K. & Lerche, I., 1993. Inversion of dynamical indicators in quantitative basin analysis models. II. Synthetic tests and a case history using dynamical indicator tomography, *Mathematical Geology,* **25,** 107–123.

APPENDIX

Let $s(t)$ be the synthetic seismogram generated by the basin simulator at a geothermal gradient of 30 °C km^{-1}, $n(t)$ is the random noise generated and $swn(t)$ is the seismogram with random noise added to $s(t)$ [$swn(t) = s(t) + n(t)$]. The random noise $n(t)$ is generated as follows:

$$n(t) = B \sum_{n=N_0}^{N_{\max}} \frac{\xi_n}{1+m} \sin\left(\frac{2\pi nt}{T} + \phi_n\right),$$

where m determines the harmonic order ranging from N_0 to $N_{\max}$, T is the total time period for the time-series, B scales the amplitude of the random noise generator according to the signal $s(t)$ and is the randomly generated phase for each Fourier component using random numbers. The parameter B is used to determine the noise level (NL). NL is related to B via

$$NL^2 = \frac{\int n^2(t)\,dt}{\int swn^2(t)\,dt}.$$